ORIGINAL PAPER

Changes in the structure of composite colloid-polymer xerogels after cold isostatic pressing

Luis Esquivias · Víctor Morales-Flórez ·
María J. Mosquera · Nicolás de la Rosa-Fox

Abstract Monolithic gels, prepared from different mixtures of colloidal silica in a sol solution containing tetraethoxysilane under powerful ultrasonic agitation (sonosols), were compacted at an isostatic pressure of 390 MPa. Then N_2 adsorption-desorption data were used to construct structural models of the gels using Monte-Carlo calculations on the basis of random close-packing (RCP) premises. Structural information on these composites obtained before compaction indicates that the characteristic uniform structure of silica colloid gel undergoes profound modification when it is mixed with silica sonogel. From a structural point of view, the behaviour under compaction of the sonogel phase, which exhibits a significant degree of microporosity, depends on the relative concentration of the colloidal phase. Two hierarchic levels of micropores were discerned. After compression, the size of the elementary particles—and their aggregates—of the sonogel phase increases from 1.6 to 2.1 nm radius when the colloidal phase content is increased from 30 to 82% by weight. For an intermediate content, 50% of the volume reduction is caused by compression of the sonogel phase at the micropore level.

L. Esquivias (✉) · V. Morales-Flórez
Departamento de Física de la Materia Condensada, Facultad de Física, Instituto de Ciencia de los Materiales de Sevilla-CSIC, Universidad de Sevilla, Avenida de la Reina Mercedes, s/n, 41012 Sevilla, Spain
e-mail: luisesquivias@us.es

M. J. Mosquera
Departamento de Química-Física, Facultad de Ciencias, Universidad de Cádiz, 11510 Puerto Real, Spain

N. de la Rosa-Fox
Departamento de Física de la Materia Condensada, Facultad de Ciencias, Universidad de Cádiz, 11510 Puerto Real, Spain

1 Introduction

It is well known that a dry gel network pressurized in a mercury porosimeter is compressed, but no mercury intrusion is observed [1–3], and the experiment produces a cold isostatic pressing (CIP) of the gel. Another significant observation from the application of porosimetry is an unexpected plastic behaviour in these gels. Pirard et al. [4] and ourselves [5] have also observed this phenomenon in xerogels. The network of a gel actually shows two different kinds of compression behaviour under isostatic pressure: the gel network is first linearly elastic under low strains, but then exhibits yield, followed by densification and plastic deformation. An important consequence of this plastic shrinkage is the possibility of densifying and stiffening these gels at ambient temperature by a simple compression process. However, in special cases, such as sonogels [5], intrusion is observed since the application of ultrasound (sonocatalysis) to the precursors gives these gels genuinely distinctive characteristics: high density, fine microporous texture, homogeneous structure, etc. [6]; these characteristics influence the behaviour of sonogels and sonogel-based composites under mechanical stresses [7].

Another special characteristic of sonogels after drying is that they present a particulate structure [8], unlike gels obtained by hydrolysis of metallorganic compounds under acid catalyst without applying ultrasound, which are filamentous. Furthermore, destabilization of colloids gives rise to gels formed by the agglomeration of the colloid particles. We have prepared crack-free monolithic SiO_2/SiO_2

Table 1 Structural parameters of the models from our catalogue employed in this study

	K_{max}	C	ρ_{RCP} (g/cm^3)	V_{RCP} (cm^3/g)	V_m (cm^3 of mesopore/g)	N_{CM}
H0L7	0.31	0.58	1.28	0.33	0.31	7.66
H0L9	0.28	0.61	1.34	0.29	0.27	8.87
H0L10	0.32	0.59	1.30	0.32	0.31	8.45

K_{max} is the distribution maximum position, C is the packing fraction, ρ_{RCP} is model specific mass in the case of being formed by silica particles; V_{RCP} is the specific volume of the model (RCP); V_m the specific mesopore volume, i.e., after subtracting the volume of the pores larger that the particle size; N_{CM} is the particle average coordination number

composites from different mixtures of colloidal silica with a sol solution containing tetraethoxysilane under powerful ultrasonic agitation (sonosol). The purpose of preparing these composites was to "fine tune" a specific structure in which the small particles generated by the sonogel process modify the uniform structure that is characteristic of the colloid gels. The colloid addition induced an increase of the pore size, involving a significant reduction of the capillary pressure during drying that favours monolith production [5]. The behaviour of these structures under mechanical stress must therefore be influenced by this microporosity existing within the sonogel phase. It is the object of this paper to describe the structural changes caused when the yield point is exceeded by cold isostatic pressing. For this purpose, Hg porosimetry runs were carried out on specimens encapsulated in rubber membranes, which prevent the entry of mercury.

The particular structural characteristic of these gels facilitates the study of their structure if an adequate strategy is applied. In this paper, as in an earlier one [9], we report structural information obtained from N$_2$ physisorption in respect of different colloid/sonogel silica composites, using models constructed with Monte-Carlo calculations, on the basis of random close packing (RCP) premises.

1.1 Structural approach

The structural approach has been fully described in previous papers [8, 9]. Essentially it consists in building models of the *solid phase* of a gel by depicting its structure as a collection of packed spherical particles [8]. Then, we created a catalogue of pore size distributions [10] according to different conditions of particle coordination number and compaction according to the features obtained from its *pore space*. The models are represented as a function of the variable $K = r/R$, where r is the radius of the largest sphere that could be inscribed in the interstice and R is the radius of the particles. Finally, pore distributions can be compared to the experimental measurement. A logarithmic scale for K is used to facilitate the fitting of the experimental data, by simply sliding it along the K axis until the position considered to give the best fit is reached. Given the

maximum, the fit allows the particle size of a mono-disperse system to be calculated from the maxima of the pore size distributions. From the distribution of each of these contributions to the experimental distribution, successive sizes and local densities of hierarchic distribution may be deduced [9]. Data on the pore volumes associated with different hierarchical levels, size of aggregates, the local density of the i-th aggregation level, and packing of the successive levels can be obtained. Table 1 gives the structural parameters of the three particular models from our catalogue used in this paper.

The whole volume enclosed by the aggregates of elementary particles, the density of the i-level, can be calculated as

$$\rho_i = \left(\sum V_i + \frac{1}{\rho_s} \right)^{-1} \tag{1}$$

where ρ_s is the elementary particle density and V_i is the pore specific volume at the i-level. Thus, we relate the measured volume to the amount of sonogel of the corresponding sample, V_i^*, in this way calculating the particular density ρ_i^* of the sonogel phase at the level i. Then, the density of the composite is calculated as the weighted average of the two phases, considering that, at this level of resolution, the density of the colloid phase is that of the bulk silica, i.e., 2.2 g cm^{-3}.

2 Experimental

2.1 Synthesis of the gels

The synthesis method is based on that proposed by Toki et al. [11], which we have already reported [5]. The sols were prepared by hydrolysis and polycondensation of tetraethoxysilane (TEOS) under acidic conditions (pH [HNO$_3$] = 1.5). A device delivering to the system 0.6 w cm^{-3} of ultrasound power was employed [12]. The total dissipated energy was 150 J cm^{-3}. Then the colloid phase was added under vigorous stirring until a homogeneous mix was obtained. The colloidal silica selected was Aerosil-OX-50 (Degussa). According to manufacturer's specifications, the product is constituted by particles of

40 nm primary average size and exhibits 50 m^2/g of specific surface area. The proportions by weight of SiO_2 colloidal particles to total SiO_2 for the various mixtures were 0, 30, 54, 65 and 82%. Each mixture was poured into hermetically-sealed receptacles and gelled at room temperature over a period of hours. Once the gelation was complete, the gels were dried in an oven at 50 °C. A pinhole aperture limited the drying rate. Gels were left in the oven until no change of weight was observed, which occurred in 2 weeks.

Monoliths from sols containing the different proportions of colloidal particles were subjected to mercury pressure, which was varied between 0.1 and 390 MPa. Cylindrical-shaped specimens ∼1.2 cm diameter and ∼1.0 cm high were encapsulated in a rubber membrane, which prevents the entry of mercury. A rotary vacuum pump was used to extract the air from the membrane. No traces of mercury were detected in the sample after weighing. Finally, the bulk densities of the gels (ρ_a) were also calculated in these experiments.

2.2 Isothermal nitrogen adsorption-desorption

The gels were texturally characterized by isothermal nitrogen adsorption-desorption at 77 K in an automatic device. Pore size distributions below 10 nm radius were calculated by the Horvath-Kawazoe (HK) method [13]. Our models will be applied to these distributions. The specific surfaces calculated by the Brunauer-Emmet-Teller (BET) method were obtained as well.

Sonogels are genuine microporous materials [14, 15]. Their microporosity was evaluated from t-plot curves [16]; this method gives the amount of adsorbed N_2 volume versus the statistical thickness during the multilayer adsorption before the capillary condensation begins. Statistical thickness, t, was calculated by the Halsey equation for a non-porous standard [17].

2.3 Electron microscopy

The composites were examined using scanning electron microscopy (SEM) and transmission electron microscopy (TEM). The observations were performed by using, respectively, the JSM 820 model installed in the Central Science and Technology of the University of Cadiz and the H800 from Hitachi installed in the Research, Technology and Innovation Center of the University of Seville (CITIUS).

3 Results

Figure 1 corresponds to an SEM micrograph of these composites. It can be seen that the structure changes from a close distribution of tiny particles, in the case of the colloid-free sample, to a uniform distribution of colloid particles coated by the sonogel phase [9].

As could be expected, the experimental gas physisorption isotherms of these samples are colloid-content

Fig. 1 SEM micrographs of samples with 0, 30, 65 and 82% by weight of colloid after isostatic compression
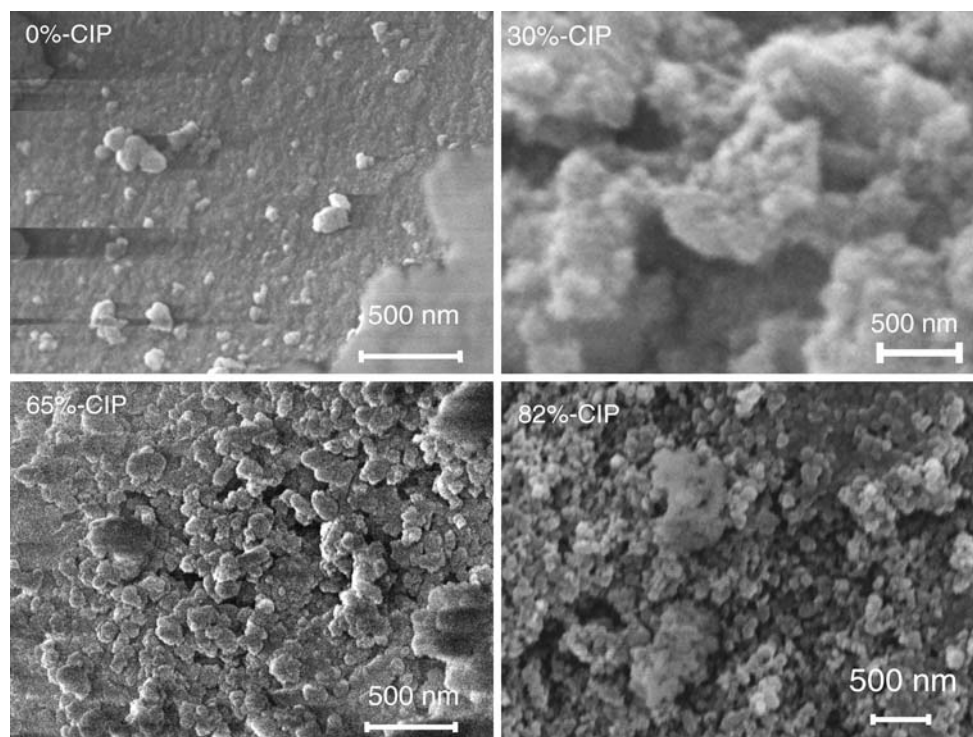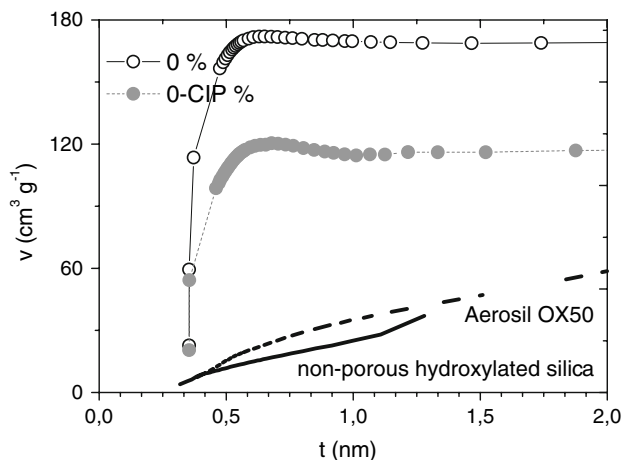
Fig. 2 Standard t-plots obtained from the experimental gas physisorption isotherm of the pure silica sonogel samples

dependent [5]. The standard *t*-plots of the pure silica sonogel (before and after compaction) are shown in Fig. 2. They present two regimes: a sharp increase of the adsorbed volume for low *t* and, as a consequence of the absence of mesopores, the curve saturates. Both curves have the same shape although the one after compression presents a uniform decrease of the micro-pore volume. The steep initial rise of the curves is a consequence of the multilayer formation and filling of the super-micropores <0.7 nm. This region can be linearly extrapolated to *t* = 0, and this slope gives an estimate of the total specific surface area. The contribution of the microporosity can be appreciated from the slope of the experimental curves in comparison with those of the standards included: a non-porous hydroxylated silica (continuous line) and the pure fumed silica Aerosil OX50 (dashed line) used in this work. Extrapolated values are similar to those calculated by the BET equation (Table 2) indicating that the main contribution to the surface area corresponds to the micropores. The decrease of the S_{BET} after compaction is mainly a consequence of the collapse of micropores.

In Fig. 3 the series of standard *t*-plots of the mixed polymer-colloidal gels under study are represented. As the content of colloidal particles increases, the saturation region changes to monotonically increasing curves with increasing *t*, and the magnitude of the step at low *t* values decreases. This is an effect of the interstitial space between the colloidal particles, the size of which is in the mesopore range.

Table 2 Experimental results of the specific surface area ($m^2 g^{-1}$) from the N_2 adsorption/desorption isotherms (77 K)

| Colloid content (% weight)	0	30	54	65	82	OX-50
Before CIP		480	392	309	226	140	60
After CIP		320	245	129	117	80	

There are differences between *t*-plots before and after the compaction as a function of the colloid content, which also require comment. The samples before compaction show the steep rise of the adsorbed volume at a lower relative pressure, indicating a higher microporous volume. As the colloid content is increased, the adsorbed volume decreases because the microporosity decreases since the sonogel phase content is lower. After compaction other features can be identified such as the linear increase between 0.5 nm < t < 1 nm due to a more homogeneous distribution of these micropores. The curves for the 30 and 54% samples exhibit changes in their shape that can be attributed to the collapse of micropores, resulting in an increased meso-porosity. This effect can be better appreciated from the increase of the slope in the second part of these curves, and is similar for t > 1 nm in both curves, before and after compaction. The collapse of micropores is more appreciable when the colloid content is higher (in the 65% sample), and the texture of the compacted 82% sample becomes closer to that of the Aerosil OX50. The final slope of the curves of the compacted 65 and 82% samples indicates the existence of a significant degree of macro-porosity.

In Fig. 4 the pore distributions of the sample without Aerosil before and after cold isostatic compression are represented. A decrease of the porosity at a radius of less than 1 nm can be observed. This cannot be fitted to one of the models of our catalogue because of the existence of a substantial degree of microporosity which overlaps the smallest pores of the next higher level of distribution. However, the particle radius can be estimated from the tail. This is because, in a random close-packing of spheres, the upper limit of the pore size is found at 0.8 < K < 1, depending on the closeness of the contact [9]. Thus, the radius of the particles, which are actually aggregates of several particles, is 2.6 nm with an estimated error of 10%. The texture that can be observed in Fig. 5 agrees with this statement.

This structural change is also featured in the case of the sample containing 30% by weight of AOX-50 (Fig. 6) since the structure at this level is entirely due to the sonogel phase. Here the decrease of the porosity at a radius of less than 1 nm is accompanied by an increase of the number of pores with radius larger than 1.5 nm, and an extension of the lower limit of micropore size. The isostatic compression has reduced super-microporosity, in agreement with our *t*-plot analysis. Thus, contrary to the case of the previously-reported uncompressed sample [9], it is possible to match the distribution for pores of less than 1 nm in radius with the model H0L9 of our catalogue. Likewise, re-structuring leads to the formation of larger elementary particles and their aggregates.
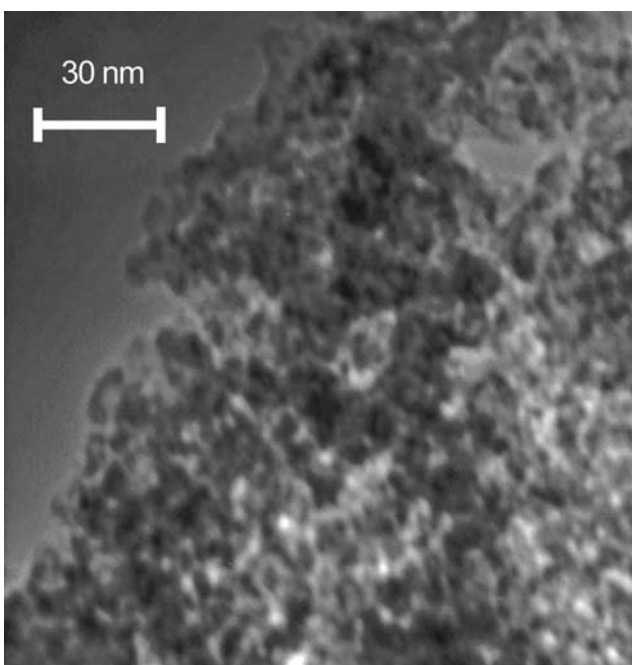
The distributions of the compressed samples can be fitted to the denser and relaxed models of our catalogue,

Fig. 3 Standard *t*-plots obtained from the experimental gas physisorption isotherm of these samples
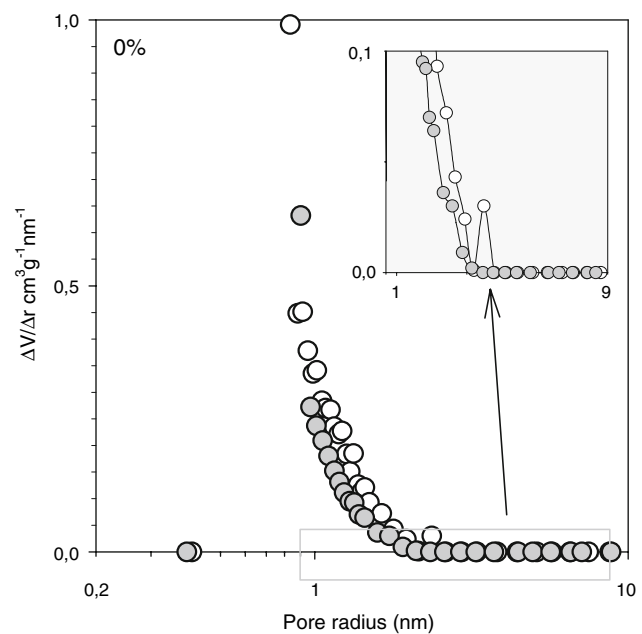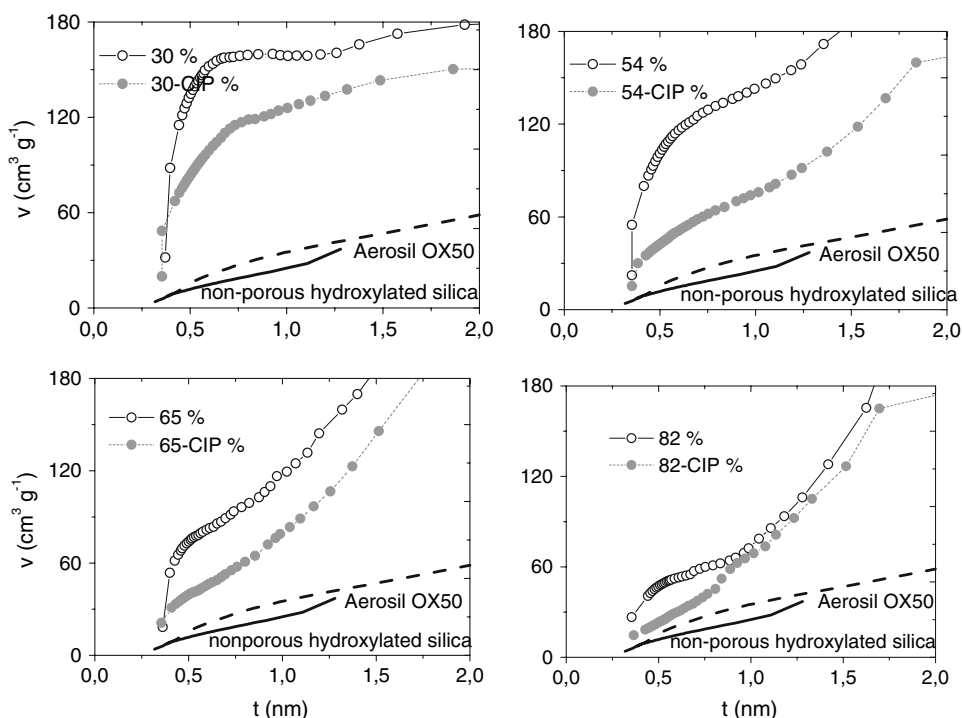
Fig. 4 Pore size derivatives of a silica sono-xerogel from TEOS. Data were obtained from N_2 adsorption-desorption before (white dots) and after (grey dots) CIP. Lines in the inset are eye-guides

Fig. 5 TEM micrograph of the pure xero-sonogel after compression

with coordination number, $\overline{CN} \sim 8$: H0L9 or H0L10 at the level of the elementary particles, and H0L7 for the structure formed by aggregates of these particles. As we have reported [9, 10], the gel structure could be arranged in several hierarchic levels. In this case, the spheres of the 1st level, of r_1 radius, are formed by a similar arrangement of smaller spheres of r_0 radius, q_1, the radius ratio being:

$q_1 = r_1/r_0$. The results of the analysis and fitting to our models are given in Table 3.

The radius of the elementary particles of the 30% sample is 1.6 nm, and these form aggregates of 4.0 nm in radius, with an estimated error of 10%. Accordingly, the structure of this sample can be described by a uniform distribution of aggregates of this size. In the former study

Fig. 6 Pore size derivatives of a silica sono-xerogel from TEOS (left) and a mixed colloid-polymer xerogel containing 30, 54, 65 and 82% by weight of Aerosil particles (right). Data were obtained from N_2 adsorption-desorption before (white dots) and after (grey dots) CIP. Lines in the inset are eye-guides
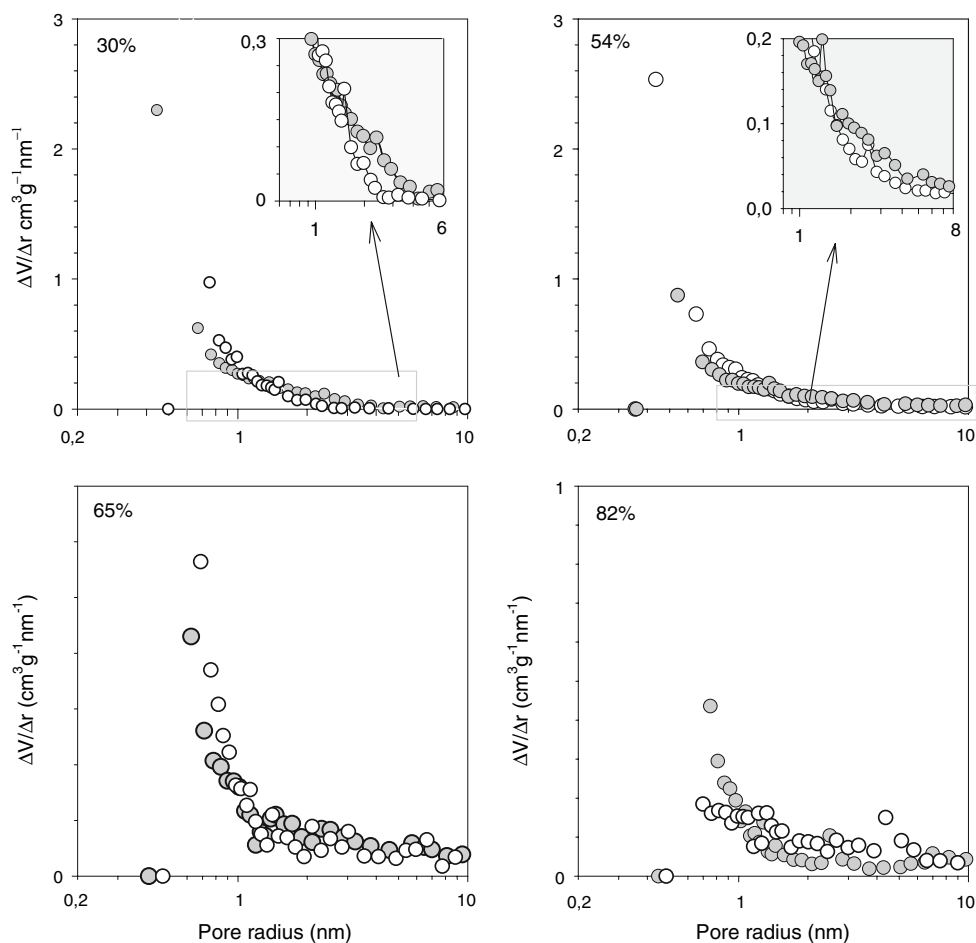
Table 3 Structural parameters of the sonogel model calculated from the models applied

Sample	Elem. particl.	Level 1						Level 2				V_{m+M}	ρ_a
	r_0	r_1	q_1	ρ_1	ρ_1*	C_1*	V_1	ρ_2	ρ_2*	C_2*	V_2		
0	–	2.6	–	1.64	1.64	0.75	0.15	1.56	1.56	0.95	0.03	0.03	1.51
0-CIP	–	2.6	–	1.63	1.63	0.73	0.16	1.53	1.53	0.94	0.04	~ 0	1.61
30	~ 1.3	4.0	~ 3	1.54	1.37	0.62	0.19	1.41	1.22	0.89	0.06	0.03	1.36
30-CIP	1.6	4.0	2.5	1.71	1.57	0.71	0.13	1.52	1.34	0.85	0.07	0.04	1.43
54	~ 1.3	4.3	~ 3.3	1.62	1.24	0.53	0.16	1.52	1.12	0.90	0.04	0.13	1.26
54-CIP	1.7	4.8	2.9	1.81	1.49	0.67	0.10	1.59	1.20	0.80	0.07	0.07	1.43
65	~ 1.3	3.9	3.0	1.76	1.29	0.50	0.11	1.67	1.16	0.90	0.03	0.31	1.11
65-CIP	1.8	5.0	2.8	1.84	1.45	0.66	0.08	1.64	1.12	0.77	0.07	0.18	1.28
82	–	Unstructured						1.67	0.80	0.37	0.14	0.44	0.97
82-CIP	2.1	–	–	1.85	1.11	0.51	0.08	1.75	0.94	0.85	0.03	0.32	1.13

r_i (nm), ρ_i (g of composite/cm^3), ρ_i*(g of sonogel/cm^3), V_i(cm^3/g of composite), $\rho_0 = 2.2$ g/cm^3, $q_1 = r_1/r_0$, ρ_a(g/cm^3)

of the structure of their uncompressed counterparts, it was not possible to resolve the pore size at the level of the elementary particles but their size was estimated from the position of the tail to be ~ 1.3 nm. The sonogel structure is identifiable in the 54 and 65% samples as well. This consists, respectively, of particles of 4.8 and 5 nm in radius

that are actually aggregates of elementary particles of 1.7 and 1.8 nm in radius. The 82% sample presents a different behaviour. The compression causes a major rearrangement of the sonogel phase, which coats the colloid particles [9]; the unstructured arrangement prior to application of isostatic pressure transforms into a RCP structure of particles

with a radius of 2.1 nm, which is correctly described by the model H0L10.

In all the cases, the ratio of particle to aggregate size is less than three, indicating that the particles penetrate each other sharing a fraction of their volumes. As we said above, the porosity at this level is due only to the sonogel structure.

4 Discussion

The structure of the pure sonogel sample consists of aggregates with a radius of 2.6 nm [9]. A compaction performed at this level results in a change of the structure, as demonstrated in the pore distributions calculated by the Horvath-Kawazoe method [13] from the N₂ adsorption-desorption experiment (Fig. 7), where the compaction caused by the collapse of pores with radius of less than 2.1 nm can be recognized.

The cross sections of the models that characterize the structure of the sonogel phase are represented in the middle. They account for the structure at the level of elementary particle aggregates before [9] and after CIP

(H0L9 and H0L7, respectively), respectively. Illustrated above each are the structures at the level of the elementary particles, which is magnified as indicated. The broken line is the proposed tail of the super-micropore distribution.

In the case of the 30% sample, the radius of the sonogel particle aggregates calculated is 4.0 nm. Yielding reduces the number of pores smaller than 1 nm, giving rise to an increase of the density at this level because the size of the elementary particles is larger but they aggregate to a more compact degree ($q_1 = 2.5$). This results in larger pores between these aggregates that increase the pore distribution from $r \sim 1.3$ nm and above, according to the model represented in Fig. 8. In our former paper [9], we showed that, in the case of the 30% sample before compaction, the network of aggregates of elementary particles matches the model H0L9 of our catalogue, whereas, according to the result presented in this paper, the structure of its compacted counterpart fits the model H0L7.

As in the preceding cases, the re-structuring induced by compression in the 54, 65 and 82% samples is caused by a decrease in the number of pores smaller than 1 nm radius and a resulting increase in the number of pores larger than 2 nm. The 82% sample deserves special comment because,

Fig. 7 Pore size derivatives at the level of the sonogel structure obtained from N₂ physisorption fitted with the models indicated. Dots correspond to the experimental output. Solid lines are the pore distribution of the models applied
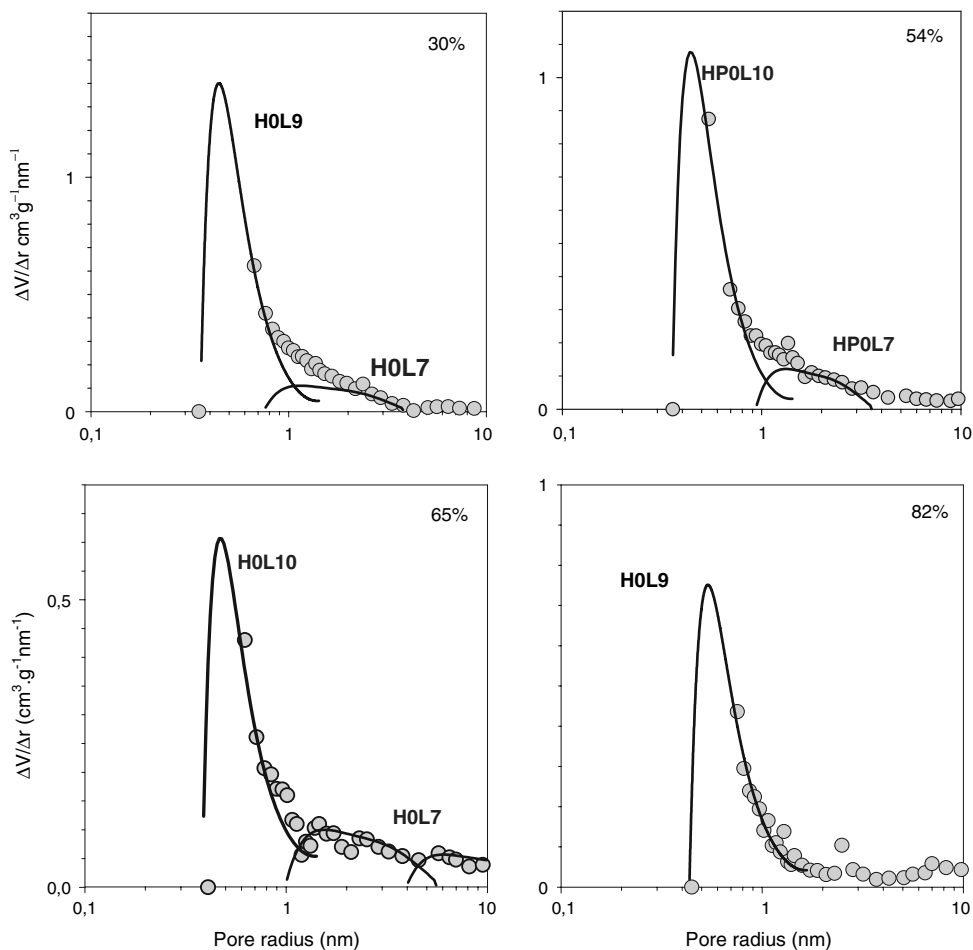
Fig. 8 Pore size derivatives at the level of the sonogel structure obtained from N_2 physisorption fitted with the models indicated, corresponding to the 30% sample (below)
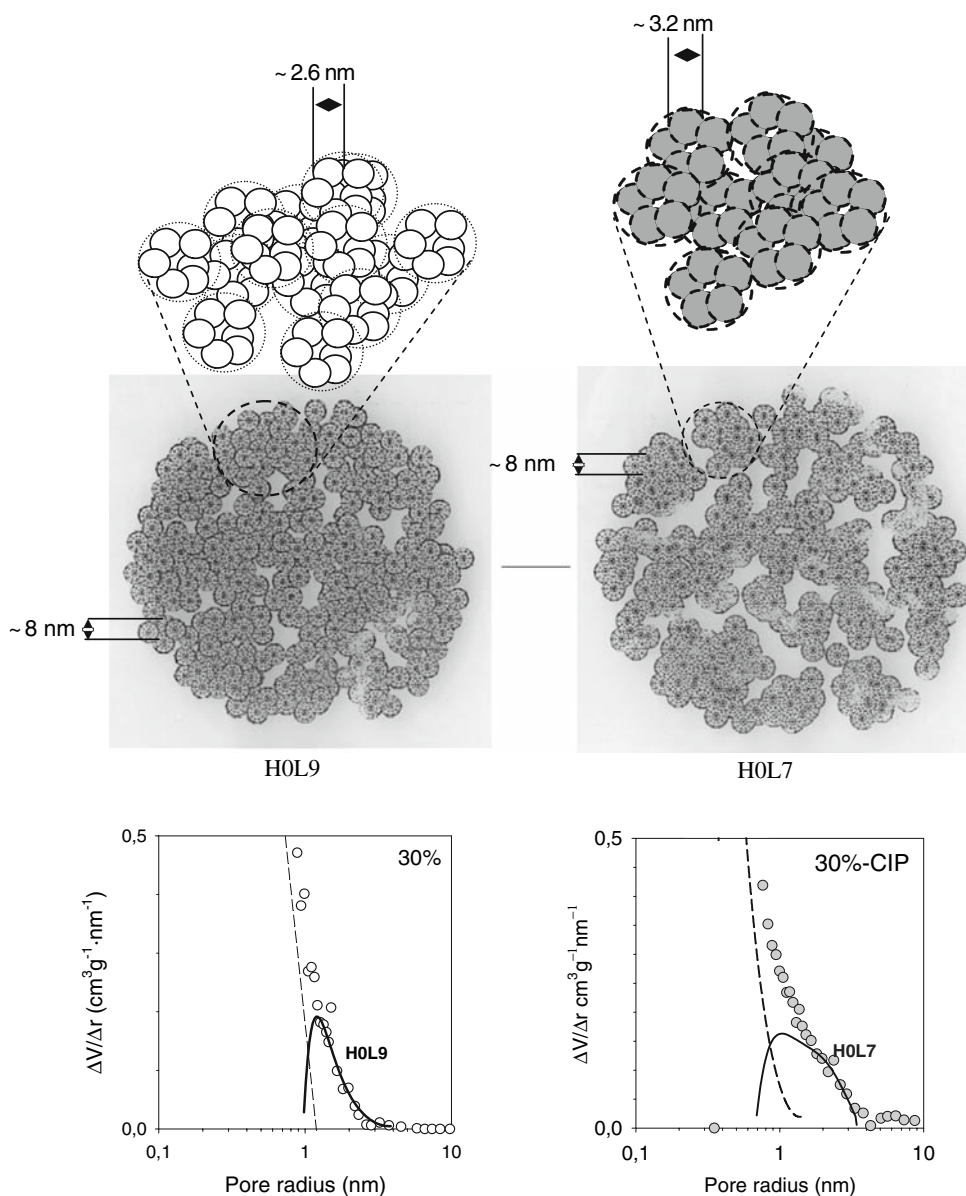
prior to compression, it is found to be unstructured at this level, but becomes well-structured once it has been compressed.

The compression causes the collapse of pores smaller than 1 nm, resulting in an increase of the particle size at the elemental level in all the cases. The radius of the elementary particle after compression depends on the colloidal particle content. It increases from a radius of ~ 1.3 nm for the uncompressed samples to gradually larger sizes of radius, from 1.6 nm for the 30% sample to 2.1 nm for the 82% sample. Consequently, the density at the level 1, which corresponds to the network of particles formed by aggregation of elementary ones, increases because of the reduction of the micropore volume (V_1). As a result, the density of the sonogel phase also decreases

with decreasing concentration of the sonogel due to the increased particle size. The differentials with respect to the initial value become greater with the Aerosil content, as well. The decrease of the packing fraction of the sonogel phase (C_1^*) also expresses this change; the network becomes looser with increasing Aerosil concentration. The packing fractions are close to that of the bcc. As these are disordered systems, under a hypothesis of perfectly spherical particles, they have to share a part of their volume with their neighbouring particles, as corresponds to q_1 values of less than 3.

The sum of V_1 and V_2 accounts for the micropore volume, and the difference with the inverse of the bulk density represents the total volume of meso- and macropores (V_{m+M}) shown in Table 3. As may be expected, the higher

the particle concentration the larger the V_{m+M}, and the greater the difference with respect to the corresponding values of the uncompressed samples.

The pure sonogel sample behaves differently from the sonogel phase in the composite. The size of the particles at the first level is at least 35% less than the corresponding counterpart of the composite samples. The density decreases both at the level of the elementary particles and the level of their aggregates. However, V_{m+M} decreases considerably, resulting in an increase of the bulk density. This indicates that the presence of the colloid particles affects the aggregation kinetics of the sonogel nuclei. The higher the colloidal particle content the larger the sonogel particles.

The yield point is related to the continuity of the sonogel phase. The pressure at which the structure deforms plastically decreases with the sonogel phase content (370, 300, 125, 125, 300 MPa for 0, 30, 54, 65 and 82% samples, respectively [5]) until the percolation threshold is exceeded, after the colloid phase occupies the gel space and takes the process over. In the case of the 82% sample the colloid particles are in almost direct contact (with almost no sonogel interface) and this favours the elastic behaviour at high pressures.

5 Conclusions

1. N_2 adsorption-desorption data were used to construct structural models of colloid polymer composite xerogels after cold isostatic pressing, on the basis of random close packing (RCP) premises.
2. The behaviour under compaction of the sonogel phase, which exhibits a significant degree of microporosity, depends on the relative concentration of the colloidal phase.
3. Two hierarchic levels of micropores were discerned.
4. The presence of the colloid particles affects the aggregation kinetics of the sonogel nuclei. The size of the elementary particles –and their aggregates- of the sonogel phase increases from 1.6 to 2.1 nm radius by increasing the colloidal phase content from 30 to 82% by weight.

5. For an intermediate content, 50% of the volume reduction is caused by compression of the sonogel phase at the micropore level.
6. The results indicate that it should be possible to "fine tune" the texture of these xerogels.

References

1. Pirard R, Blancher S, Brouers F, Pirard JP (1995) J Mater Res 10:1
2. Duffours L, Woignier T, Phalippou J (1995) J Non Cryst Solids 186:321
3. Scherer GW, Smith DM, Qiu X, Anderson J (1995) J Non Cryst Solids 186:316
4. Pirard R, Heinrichs B, Van Cantfort O, Pirard JP (1998) J Sol-Gel Sci Technol 13:335
5. Mosquera MJ, Bejarano M, de la Rosa-Fox N, Esquivias L (2003) Langmuir 19:951
6. Esquivias L, Rodríguez-Ortega J, Barrera-Solano C, de la Rosa-Fox N (1999) J Non-Cryst Solids 225:239
7. de la Rosa-Fox N, Esquivias L, Zarzycki J (1987) Diffusion Defect Data 53/54:363
8. Rodríguez-Ortega J, Esquivias L (1997) J Sol-Gel Sci Technol 8:117
9. Esquivias L, de la Rosa-Fox N, Bejarano M, Mosquera MJ (2004) Langmuir 20:3416
10. Rodríguez Ortega J (1996) PhD thesis, University of Cádiz, Cádiz, Spain
11. Toki M, Miyashita S, Takeuchi T, Kanbe S, Kochi A (1988) J Non-Cryst Solids 100:479
12. Esquivias L and Zarzycki J (1986) Current topics on non-crystalline solids. In: Baró MD, Clavaguera N (eds) World Scientific, Singapore, pp 409–414
13. Horvath G, Kawazoe K (1983) J Chem Eng of Japan 16(6):470
14. Zarzycki J (1994) Heterogeneous Chem Rev 1:243
15. Blanco E, Esquivias L, Litran R, Piñero M, Ramírez-del-Solar M, de la Rosa-Fox N (1999) Appl Organomet Chem 13:399
16. Lowell S, Shields JE (1984) Powder surface area and porosity. Chapman and Hall, New Cork, Chapter 9
17. Halsey G (1948) J Chem Phys 16:931